

RESEARCH

Open Access



# DenMerD: a feature enhanced approach to radar beam blockage correction with edge-cloud computing

Qi Liu<sup>1,2\*†</sup>, Jiawei Sun<sup>2†</sup>, Yonghong Zhang<sup>3</sup> and Xiaodong Liu<sup>4</sup>

## Abstract

In the field of meteorology, the global radar network is indispensable for detecting weather phenomena and offering early warning services. Nevertheless, radar data frequently exhibit anomalies, including gaps and clutter, arising from atmospheric refraction, equipment malfunctions, and other factors, resulting in diminished data quality. Traditional radar blockage correction methods, such as employing approximate radial information interpolation and supplementing missing data, often fail to effectively exploit potential patterns in massive radar data, for the large volume of data precludes a thorough analysis and understanding of the inherent complex patterns and dependencies through simple interpolation or supplementation techniques. Fortunately, edge computing possesses certain data processing capabilities and cloud center boasts substantial computational power, which together can collaboratively offer timely computation and storage for the correction of radar beam blockage. To this end, an edge-cloud collaborative driven deep learning model named DenMerD is proposed in this paper, which includes dense connection module and merge distribution (MD) unit. Compared to existing models such as RC-FCN, DenseNet, and VGG, this model greatly improves key performance metrics, with 30.7% improvement in Critical Success Index (CSI), 30.1% improvement in Probability of Detection (POD), and 3.1% improvement in False Alarm Rate (FAR). It also performs well in the Structure Similarity Index Measure (SSIM) metrics compared to its counterparts. These findings underscore the efficacy of the design in improving feature propagation and beam blockage accuracy, and also highlights the potential and value of mobile edge computing in processing large-scale meteorological data.

**Keywords** Mobile edge computing, Radar beam blockage correction, Image restoration, Deep learning

## Introduction

Weather radar, as an active remote sensing instrument, employs electromagnetic waves to ascertain precipitation location and intensity. Contemporary weather radar offers high spatial and temporal resolution data, proving valuable for meteorological services [1–3]. Due to atmospheric refraction, equipment failure and other factors, radar echoes can suffer from beam blockage [4, 5]. Filling in the correction of radar beam blockage and achieving radar data quality control can effectively improve disaster prevention and mitigation capabilities under extreme weather conditions, and strongly guarantee the safety of, for example, maritime transport and aviation.

<sup>†</sup>Qi Liu and Jiawei Sun contributed equally to this work.

\*Correspondence:

Qi Liu  
qi.liu@nuist.edu.cn

<sup>1</sup> Jiangsu Province Engineering Research Center of Advanced Computing and Intelligent Services, Nanjing University of Information Science and Technology, Nanjing 210044, China

<sup>2</sup> School of Software, Nanjing University of Information Science and Technology, Nanjing 210044, China

<sup>3</sup> School of Automation, Nanjing University of Information Science and Technology, Nanjing 210044, China

<sup>4</sup> School of Computing, Edinburgh Napier University, Edinburgh EH10 5DT, UK

Traditional methods for addressing weather radar beam blockage involve leveraging the radar's actual position and the angle of the data-deficient region at the same or neighboring elevations, accompanied by manual observation of data patterns, rule design, model customization, and subsequent data supplementation based on adjacent information [6]. A sophisticated quality control algorithm has been developed for dual PRF radial velocity data, comprising noise isolation based on echo size, deblurring via local continuity, and targeted singular value adjustments to rectify inherent data errors [7]. Concurrently, an innovative correction method using averaged reflectivity factor vertical profiles has been employed to mitigate radar beam blockage effects, significantly enhancing quantitative precipitation estimation accuracy in obstructed regions [8].

Despite the efficacy of traditional interpolation and data-filling approaches in performing beam blockage correction, these methods are relatively inefficient and limited due to the fact that they do not take advantage of the superb arithmetic power of the big data era, which makes them limited in taking full advantage of the deep regularities that exist in a wide range of weather radar data. In recent years, deep learning has found widespread applications across various domains such as computer vision, edge computing, anomaly detection, and data mining, yielding remarkable results [9–14]. The training of deep learning models is an intensively resource-dependent task, necessitating substantial computational capabilities and storage capacity [15–19]. Mobile Edge Computing (MEC) utilises the computational resources of edge devices to save energy consumption for smart devices and reduce computational latency of tasks, while avoiding network congestion in traditional cloud computing. Therefore, many researchers have worked on the application of MEC in different scenarios [20–25]. The challenge presented by radar beam blockage correction is manifested as a distortion or deficiency in the radar echo images. This observation implies that a potential solution could be explored through the application of image restoration methods, which are designed to rectify and enhance visual data integrity in similar contexts. In the realm of image restoration, deep learning methodologies have advanced rapidly and achieved substantial progress. However, the application of such techniques in radar beam blockage correction research remains relatively unexplored. The potential for applying these techniques to radar beam blockage correction is considerable and anticipated to yield superior revision outcomes.

The main contributions of this paper are summarised as follows:

- An edge-cloud collaboration deep learning radar beam blockage correction approach is proposed, which effectively improves the radar big data processing efficiency and beam blockage correction accuracy.
- A radar beam blockage correction deep learning model is designed, which includes dense connection module and merged distribution transition unit. Compared with other advanced models, the proposed model has better correction performance.
- The beam blockage correction experiments in this paper are carried out on two datasets based on the radar echo data of Guangzhou Station and achieve good results in the evaluation metrics in the fields of meteorology and image restoration, such as CSI, POD, FAR and SSIM.

The rest of the paper is presented as follows: The [Related work](#) section discusses relevant research advances in radar beam blockage correction. The [Method](#) section discusses the system model proposed in this paper, the cloud depth model and the important components of it. The [Experiments](#) section discusses the production of the dataset, the evaluation metrics, the loss function and the experimental results. The [Conclusion](#) section summarises the findings of the work in this paper.

### Related work

This section discusses the research status of radar beam blockage and the related research progress of image restoration, and briefly introduces how to solve the related problems in this paper.

### Traditional beam blockage correction methods

Currently, there are two main types of radar beam blockage revision methods, one that relies on terrain data and another that does not. Terrain data, specifically the Digital Elevation Model (DEM), encompasses the elevation information of terrain grid points. Zhang et al. [26] utilized the distance bank mean fill method pertaining to DEM data, utilizing neighboring Plan Position Indicator (PPI) echo information, to ascertain real-time correction factors that enable the revision of sparse smaller radial blockages. Chen et al. from [27] used DEM data from the Shuttle Radar Topography Mission (SRTM) and DEM data from Google to calculate the beam blockage rate at low elevation angles of S-band radars located in the southern suburbs of Beijing, respectively, and established a revised relationship for the echo reflectivity in partially blocked areas. Liu et al. [28] used SRTM digital elevation data to simulate and calculate the beam occlusion of 212 new generation weather radars currently operating in China.

These methods depend on topographic information, and due to rapid high-rise construction accompanying societal development, it becomes challenging for topographic data to be promptly reflected in DEM data, consequently impacting data revision accuracy. Gou et al. [29] used the method of first removing the partially blocked radar echoes and then revising the discontinuity effect caused by partial blockage by re-gridding the puzzle. Huang et al. [30] proposed a beam blockage identification and revision algorithm that does not rely on a superior accuracy DEM. The algorithm performs blockage identification first and then linear interpolation for the inaccurate echo data caused by partial blockage or small-area complete blockage to achieve the revision of the blockage data. Wang et al. [31] analysed the climatic characteristics of the frequency of radar echoes of different intensities and their spatial distribution and other characteristics from the perspective of radar climate statistics, based on which the radar clutter was identified and revised.

Although these two types of traditional beam blockage correction methods have achieved some results, these manual interpolation methods based on neighbouring contexts fail to exploit the superb arithmetic power of the big data era to mine the potential laws of massive radar data, which leads to inefficient beam revision.

#### **Advanced deep learning approaches for image restoration and radar beam blockage correction**

As deep learning techniques have evolved in contemporary studies, a variety of deep learning approaches have been extensively employed in image restoration tasks. Mao et al. [32] proposed a single image restoration method for generative adversarial networks based on a self-attentive mechanism, incorporating WGAN to ensure comprehensive coherence of the restored region through the learning of generative adversarial models. The proposed model employs the earth moving distance to quantify the resemblance amidst a pair of distributions. Phutke et al. [33] suggested computationally efficient, lightweight networks for image restoration with minimal parameters and without guidance information. Ma et al. [34] presented a versatile restoration framework capable of addressing incomplete images exhibiting considerable missing regions, encompassing both continuous and discontinuous areas. Region operations are implemented in the generator and discriminator, catering to distinct region types specifically, existing and missing regions. Quan et al. [35] proposed a novel three-stage restoration framework encompassing local and global refinement. An encoder-decoder network with skip connections is initially utilized for generating coarse preliminary results. Aishwarya et al. [36] utilized

two adversarial networks for this task, the first targeting restoration and the second super-resolution. In order to make the image of the restored region enhanced smoothness and increased definition, Nazeri et al. [37] introduced a new image restoration algorithm facilitating the accurate recovery of missing regions. Experimental outcomes demonstrate that this approach surpasses previous methodologies in terms of both speed and quality. Hong et al. [38] approached image restoration from the unique perspective of generating a seamless transition, devising a streamlined DFNet.

Considering radar beam blockage correction as an image restoration issue, the obstructed area can be perceived as the image's covered portion. Consequently, the algorithm's objective is to discover the interrelation of data within obstructed and recognized areas in extensive radar datasets. This allows for the estimation of the pixel value with the highest probability of occurrence for each pixel point in the blocked region, which corresponds to the image's missing area. Wu et al. [39] proposed a deep learning network to correct the weather radar beam revision, on the basis of which [40] proposed an edge assisted cloud framework in which individual site radar echo signals could be analysed and pre-processed at the edge and then trained in the cloud using elastic resources and distributed learning capabilities, a RC-FCN for beam blockage revision was suggested, integrated into the framework, and compared with alternative deep learning models.

Overall, mobile edge computing and deep learning techniques have made great progress in recent years [41–46]. Therefore, applying similar techniques to beam blockage correction has great potential and is expected to achieve better correction results. The focus of this paper is to introduce the concept of mobile edge computing and adopt an edge-cloud cooperative approach to correct radar data loss due to various reasons.

## **Method**

### **System model**

In this paper, the proposition of integrating radar stations as mobile edge nodes is articulated as a cornerstone for the advancement of edge computing frameworks. This integration is especially critical for the initial processing of data procured from radar systems. Such a preprocessing phase is crucial in the data handling sequence, involving a sophisticated method of minimizing and transmuted the extensive radar data. This procedure effectively extracts and condenses the fundamental attributes required for subsequent analytical computations. Following this phase, the processed data is transmitted to an advanced, cloud-based deep learning architecture for

intensive training. This rigorous analytical undertaking is indispensable for the development and enhancement of predictive models, focusing specifically on the improvement of algorithms related to beam blockage correction. This method highlights the critical role of edge computing in enhancing both the precision and the efficiency of data processing within radar systems. It exemplifies the transformative potential that edge computing holds for advancing predictive modeling in this field.

Upon the completion of this training paradigm, the elaborately constructed model is then disseminated from the cloud to the aforementioned edge nodes. This transfer equips the nodes with the capability to execute beam blockage corrections in a decentralized manner, leveraging the computational power embedded at the edge of the network. The integration of such a system underscores the inherent efficiency and reliability that edge computing confers upon meteorological services, as it enables the swift processing of large-scale datasets pertinent to meteorological analysis. The deployment of this architecture, as depicted in Fig. 1, represents a significant shift in the methodology of processing meteorological data. It serves as a prime example of the substantial influence and essential usefulness of mobile edge computing in the handling and analysis of extensive meteorological datasets across various applications.

**Overall pipeline in cloud**

The pre-processed datasets, procured from each designated mobile edge site, are systematically relayed to a centralized cloud computing facility. This transmission is orchestrated in such a manner that it facilitates the amalgamation and synchronization of data from disparate geographic locales. Upon the arrival at the cloud centre server, this data then serves as the foundational bedrock upon which sophisticated model training is conducted. The model proposed in this paper is bifurcated into two distinct segments: encoding and decoding frameworks. The encoding framework incorporates the concept of dense connectivity to facilitate learning of more feature mappings and contains three dense connection modules. The decoding framework utilizes the upsampling structure similar to that in U-net to restore the image size.

The initial input is a  $360 \times 250$  radar echo map to be restored, resized to  $224 \times 224$ , and subsequently processed by the encoder after one convolution with a  $7 \times 7$  convolution kernel, a stride of 2, and padding of 3. It then proceeds through three dense connection modules with five transposed convolutions, all with a  $3 \times 3$  convolution kernel, a stride of 2, and no padding. Finally, the image size is restored to  $360 \times 250$  by an adaptive pooling operation, and the output of each layer of the decoder section is passed to the MD transition unit for pooling operation and then through the fully connected layer, with the final output being the restored radar echo map. The specific

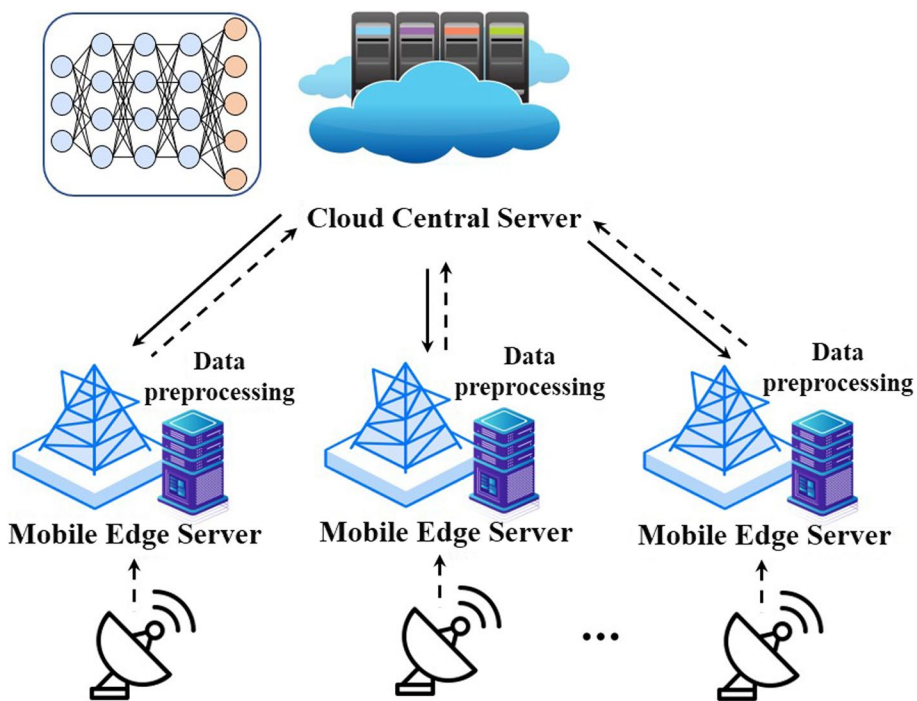


**Fig. 1** System model

architecture is depicted in Fig. 2. Through this methodical and rigorous training, the model progressively learns and adapts, effectively encapsulating the complex patterns and variances inherent in the meteorological data.

**Dense connection module**

Within the scope of this paper, the architecture of the proposed model incorporates a robust configuration of dense connectivity within its encoder segment. These modules are specifically designed to enhance the flow of information and gradients throughout the network, thereby significantly improving the model’s ability to capture and encode complex data representations.

In this network structure, each layer establishes direct connections with all previous layers, receives additional input data from them, and passes its own feature mapping to all subsequent layers.

This design employs a cascading approach that helps to transfer collective knowledge from the previous layers in

the network. This densely connected structure helps to overcome the gradient vanishing problem as each layer can more easily access gradient information from the previous layer, thus enhancing feature propagation. In addition, this design also reduces the number of model parameters relative to the traditional network structure because the layers are more tightly connected. The specific architecture is depicted in Fig. 3.

**Merge-distribution transition unit**

In the domain of meteorology, particularly in the context of radar beam blockage correction tasks, the utilization of information harvested from various levels of preceding convolutional layers is of paramount importance. Acknowledging this, the paper introduces an innovative structural component termed the Merge-Distribution (MD) transition unit. This unit is ingeniously crafted to amalgamate and distribute information more efficiently across the temporal

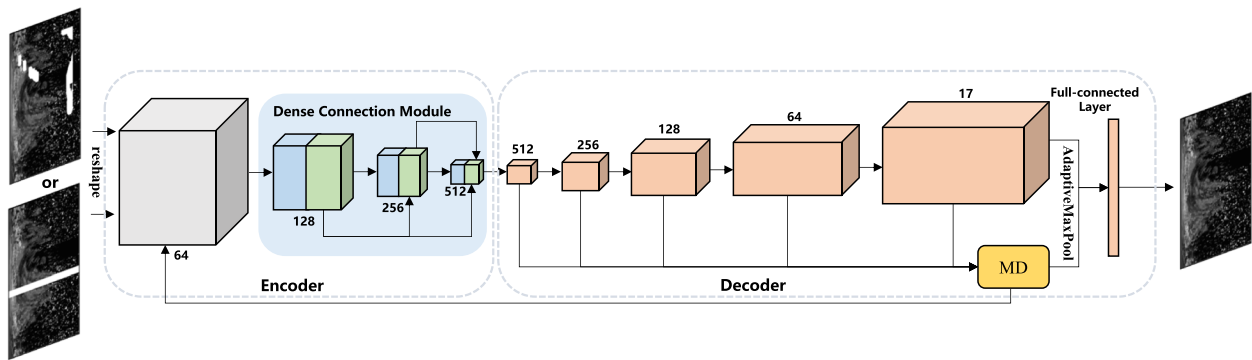


Fig. 2 Structure of the overall pipeline in cloud

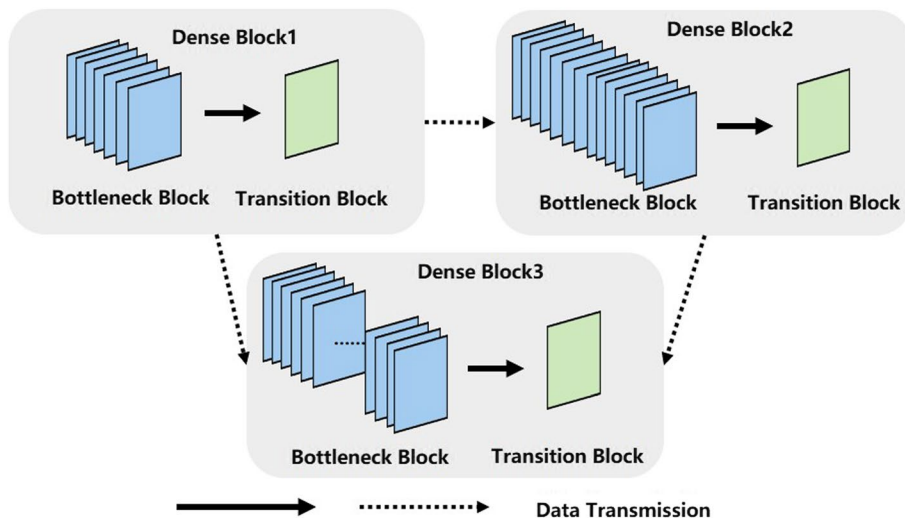


Fig. 3 Structure of the dense connection module

dimension. The primary objective of the MD transition unit is to augment the existing informational paradigm by incorporating additional inputs derived from prior temporal states, thus substantially enriching the feature propagation mechanism within the multi-layer convolutional neural network architecture. The introduction of such a unit is intended to significantly bolster the resilience and accuracy of the model by enabling a more nuanced and comprehensive synthesis of information, thereby ensuring a more robust feature representation that is vital for the precise adjustment of beam blockage phenomena in weather radar systems. This innovative approach underscores a pivotal advancement in enhancing the convolutional neural network’s ability to discern and adapt to the complex dynamics inherent in meteorological data processing.

Specifically, the MD transition unit takes the following steps to achieve this goal: First, it concatenates the output results of multiple convolutional layers, which means that these outputs are connected in one dimension to be represented by rich features. Next, this concatenated feature vector is passed to a convolution layer with a kernel size of  $1 \times 1$ , which helps to further integrate and refine the features. The output of this convolutional layer is then pooled to reduce the feature dimension and extract the most significant feature information. Finally, the processed output is passed to the convolution layer at the next time step to ensure that the new feature information can be propagated and utilized throughout the network. The specific architecture is depicted in Fig. 4.

## Experiments

### Experiment details

Mobile edge devices generate massive amounts of radar data, which are pre-processed at the edge end. In this paper, two radar echo datasets were created, both derived from aggregated reflectance images from the Guangzhou station. In order to achieve a more accurate beam blocking correction and also to provide the necessary features for the deep learning model, a series of preprocessing steps on the raw data were performed. First, the array of raw pixel values were converted into an array of radar echo strength dBZ values, and denoising and interpolation were performed considering the presence of noise values beyond the grey scale range in the aggregated reflectance images from the Guangzhou station. Each pixel in the array was determined whether it belongs to the set of grey values, and if not, mark it as an outlier and replace and fill it with the largest element in its upper, lower, left and right neighbourhood. Points with values less than 10 dBZ and greater than 70 dBZ typically represent non-meteorological clutter, so these values were replaced with zeros to prevent any detrimental effect on the model’s modelling of the effective echoes. After the denoising and interpolation operations were completed, the raw image data were converted to greyscale format to reduce computational complexity. Then, the image were expanded into a rectangular representation along the radius. Finally, randomly generated rectangles and irregular masks were manually applied on the processed images. The associated process is shown in Algorithm 1.

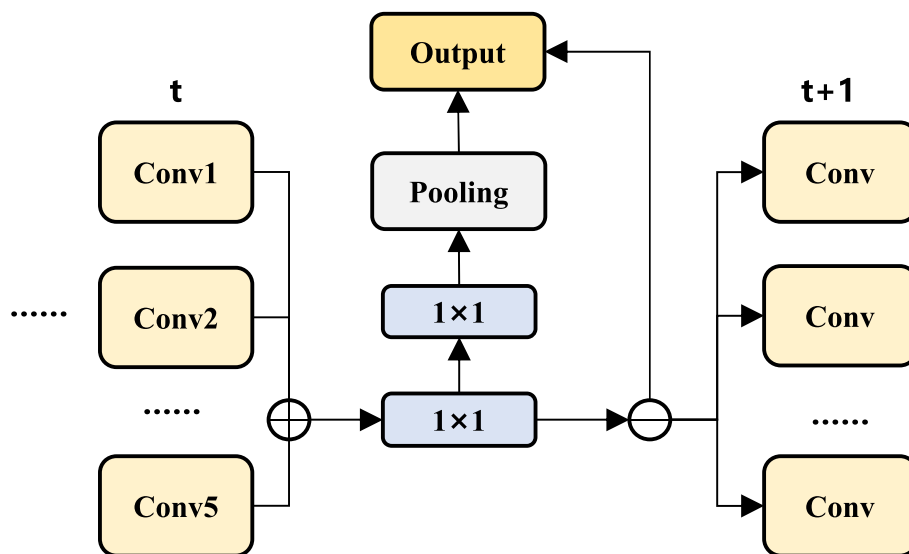


**Fig. 4** Structure of the MD transition unit

### Algorithm 1 Main steps of data preprocessing

---

**Input:** raw data.  
**Output:** rectangular grayscale image,  $(T'_{360 \times D}, T_{360 \times D})$ .

- 1: Convert the array of raw pixel values into an array of radar echo strength dBZ values,  $I$
- 2: Denoising and interpolation of the composite reflectance image of the Guangzhou station
- 3: **if**  $i \notin I_{grey}$  **then**
- 4:      $i = \max(i_{upper}, i_{lower}, i_{left}, i_{right})$
- 5: **end if**
- 6: **if**  $i < 10 \parallel i > 70$  **then**
- 7:     Set  $i = 0$
- 8: **end if**
- 9: Convert raw image data to grayscale format
- 10: **return**  $(T'_{360 \times D}, T_{360 \times D})$

---

In this way, two datasets were obtained: one containing 12,000 radar echo images with random rectangular masks, of which the first 10,000 were used as a training set and the remaining 2,000 were used as a test set; and the other containing 2,000 radar echo images with random irregular masks, of which the first 1,600 were used as a training set and the remaining 400 were used as a test set. An example of the home-made dataset is shown in Fig. 5. Radar echo image with random rectangular mask on the left and radar echo image with random irregular mask on the right.

This paper approaches the weather radar echo blockage revision issue as an instance of an image restoration problem, aiming to uncover the distribution relationship between data in the blockage and known regions within radar big data. This is carried out to estimate the pixel value exhibiting the highest probability of occurrence for each pixel point in the blockage region, which corresponds to the missing portion of the image. A multi-classification cross-entropy loss function is employed to compute the most probable pixel value for each pixel point within the area to be restored. This step can be formulated as Eq.(1):

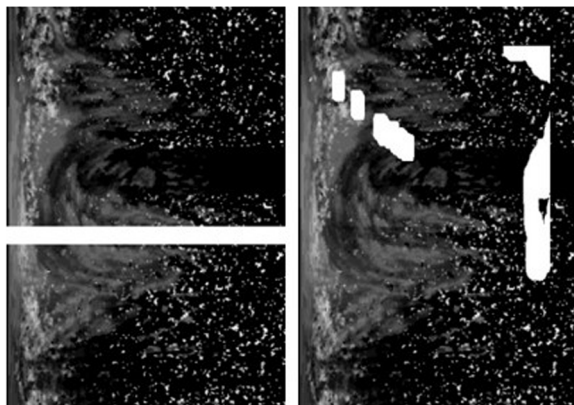


**Fig. 5** Example graph of datasets

$$Loss(z, c) = -z[c] + \log\left(\sum_{j=0}^{c-1} \exp(z[j])\right) \quad (1)$$

where  $z$  represents the predicted pixel value,  $c$  denotes the sample label, and  $z[c]$  is negative log likelihood loss. After calculating a pixel's loss, the total loss is obtained by summing the losses of all pixels within the region to be repaired.

### Evaluation metrics

The experiments conducted in this paper entail the comparison of all pixel points and the calculation of accuracy within the image restoration domain, utilizing SSIM [40] as the evaluative criterion. The calculation formula is demonstrated in Eq.(2):

$$SSIM(x, y) = \frac{(2\mu_x\mu_y + c_1)(2\sigma_{xy} + c_2)}{(\mu_x^2 + \mu_y^2 + c_1)(\sigma_x^2 + \sigma_y^2 + c_2)} \quad (2)$$

where  $x$  denotes the true input image,  $y$  signifies the restored image,  $\mu_x$  and  $\mu_y$  represent the means of  $x$  and  $y$  respectively, and  $\sigma_x$  and  $\sigma_y$  correspond to the standard deviations of  $x$  and  $y$  respectively.  $\sigma_{xy}$  symbolizes the covariance of  $x$  and  $y$ , while  $c_1$  and  $c_2$  are constants employed to prevent systematic errors due to a zero denominator.

Nonetheless, since the radar echo revision problem primarily concerns the meteorological domain, this paper also incorporates the Critical Success Index (CSI [2]), False Alarm Ratio (FAR [2]), and Probability of Detection (POD [2]) as evaluation metrics to assess the model's restoration effectiveness. The corresponding calculation equations can be found in Eq.(3), Eq.(4), and Eq.(5):

$$CSI = \frac{TP}{TP + FP + FN} \quad (3)$$

$$FAR = \frac{FP}{TP + FP} \quad (4)$$

$$POD = \frac{TP}{TP + FN} \quad (5)$$

where  $TP$  is a hit,  $FP$  is a false alarm and  $FN$  is a missed alarm.

### Experiment results

As demonstrated in Fig. 6, the radar echo image beam revision effect of the proposed model can be visualized. Regarding the area of the image to be restored, the model

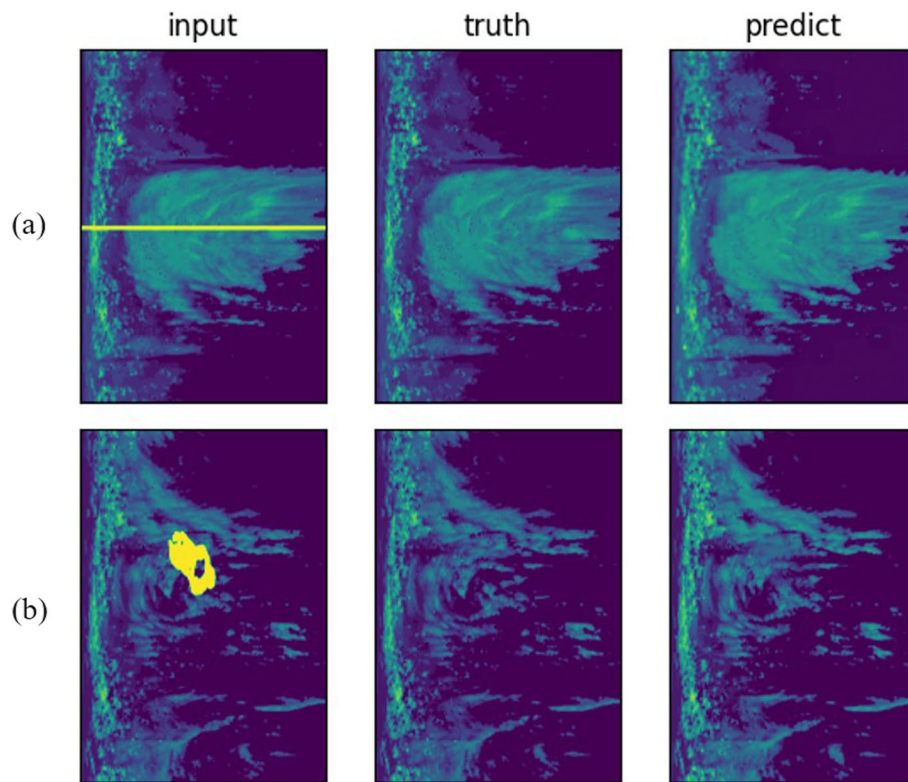


**Fig. 6** Example of restored image with beam blockage

yields satisfactory outcomes, in terms of both overall image external contours and specific detail levels.

Accuracy is used to describe the pixel-level difference between the predicted image and the true value and measures the performance of the model. As shown in Figs. 7 and 8, the accuracy of the beam blockage revision of the proposed model has been improved compared to VGG, DenseNet, DFNet and RC-FCN. These models are chosen in this paper because the model proposed in this paper use encoding and decoding structures and contain modules such as dense connection, and these model structures are also relevant. Therefore, by comparing with these models, the improvement of the model proposed in this paper in terms of beam blockage correction accuracy can be more comprehensively assessed and demonstrated.

The proposed model incorporates encoding and decoding frameworks, complemented by the dense connection module and MD transition unit. Quantitative comparisons with VGG, DenseNet, DFNet, and RC-FCN are performed. The detailed results are exhibited in Tables 1, 2, 3, and 4, with the top results

displayed in bold and the runner-up results underlined. In the evaluation metrics used in this paper, higher values of CSI, POD, and SSIM represent better model performance, and lower values of FAR represent better model performance.

Under the CSI evaluation metric, DenMerD excels in most dBZ value ranges in the Rectangular Mask dataset, improving 17.4%, and 30.1% relative to the next best models, RC-FCN, and VGG, respectively. This highlights the effectiveness of the dense connection module and MD transition unit in enhancing feature propagation in DenMerD. In the Irregular Mask dataset, DenMerD also shows excellent performance, improving 14.6% and 30.7% with respect to the second-best models RC-FCN and VGG, respectively, which further validates the usefulness of these modules.

Under the FAR evaluation metric, DenMerD improves 3.1% and 2.2% relative to the second-best model in the 45-50 and 35-40 dBZ value ranges, respectively. These boosts can be traced back to DenMerD's dense connection module, which helps to propagate feature information more efficiently and improve model performance.

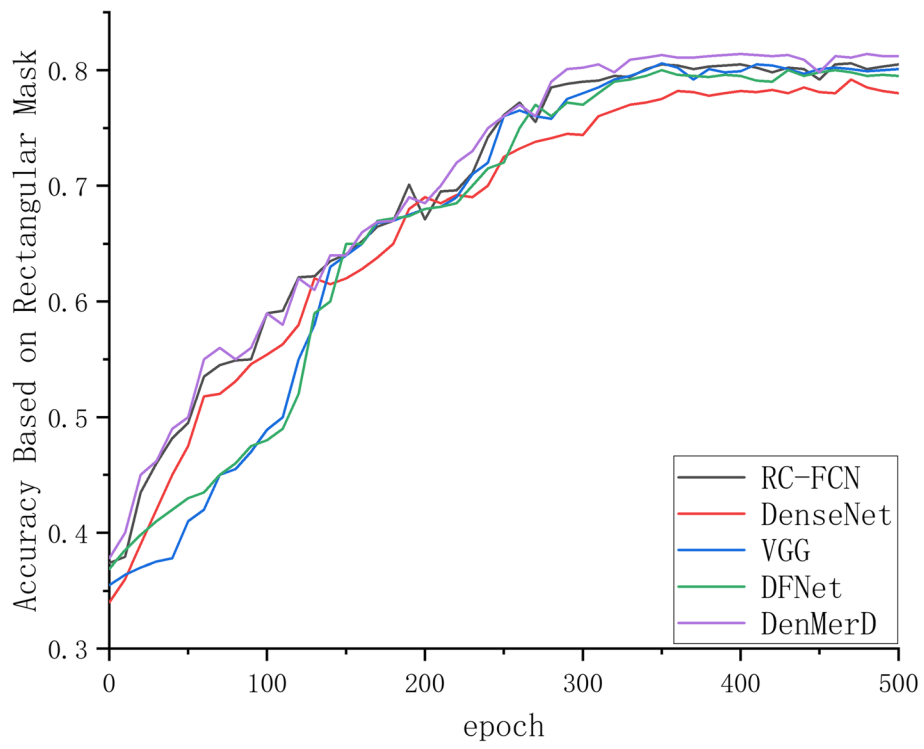


Fig. 7 Accuracy based on rectangular mask

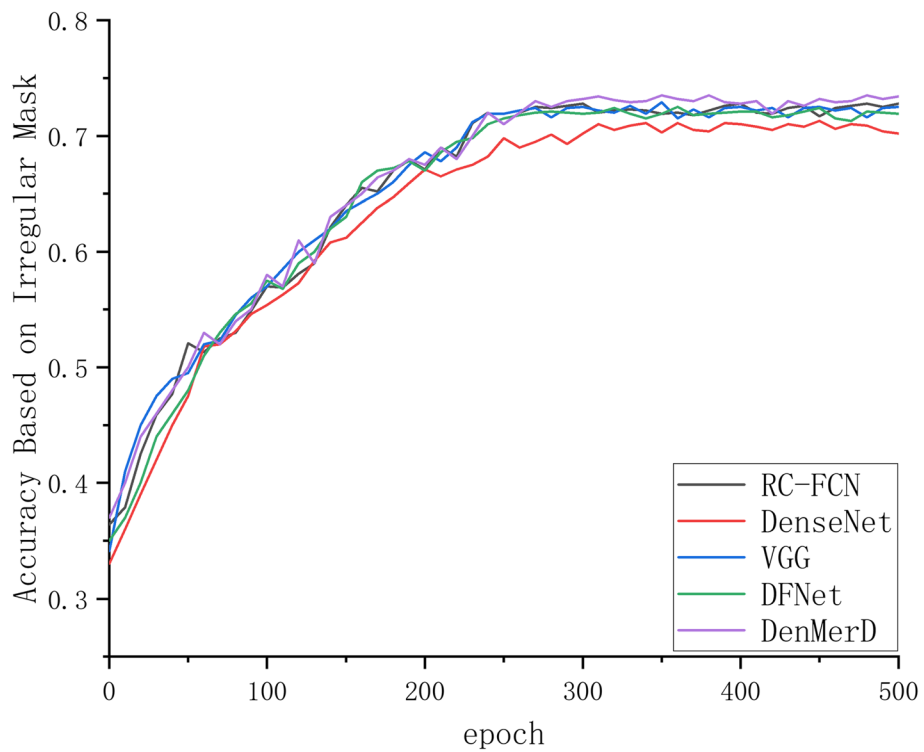


Fig. 8 Accuracy based on irregular mask

**Table 1** A comparative assessment of CSI

| dBZ   | Dataset          | VGG           | DenseNet      | DFNet         | RC-FCN        | DenMerD*      |               |
|-------|------------------|---------------|---------------|---------------|---------------|---------------|---------------|
| 55-60 | Rectangular Mask | 0.0141        | <u>0.0152</u> | 0.0144        | 0.0133        | <b>0.0308</b> |               |
| 50-55 |                  | 0.0724        | 0.0641        | 0.0647        | <u>0.0736</u> | <b>0.0864</b> |               |
| 45-50 |                  | <u>0.1938</u> | 0.1325        | 0.1722        | 0.1065        | <b>0.2521</b> |               |
| 40-45 |                  | <u>0.1916</u> | 0.1489        | 0.1323        | 0.1122        | <b>0.2101</b> |               |
| 35-40 |                  | 0.1777        | 0.1351        | 0.1745        | <u>0.1802</u> | <b>0.1912</b> |               |
| 30-35 |                  | 0.2291        | 0.1825        | 0.1691        | <u>0.2368</u> | <b>0.2563</b> |               |
| 25-30 |                  | 0.2001        | 0.1629        | 0.1982        | <u>0.2052</u> | <b>0.2246</b> |               |
| 20-25 |                  | 0.1362        | 0.1945        | 0.136         | <u>0.2181</u> | <b>0.2215</b> |               |
| 15-20 |                  | <u>0.2015</u> | 0.1903        | 0.1589        | 0.1046        | <b>0.2134</b> |               |
| 10-15 |                  | 0.2352        | 0.2238        | 0.2563        | <b>0.2675</b> | <u>0.2517</u> |               |
| 5-10  |                  | 0.2974        | 0.3011        | 0.3029        | <b>0.4102</b> | <u>0.3133</u> |               |
| 0-5   |                  | 0.2643        | <u>0.2689</u> | 0.2692        | 0.2663        | <b>0.2759</b> |               |
| -20-0 |                  | 0.3541        | 0.3612        | 0.3614        | <b>0.4387</b> | <u>0.3728</u> |               |
| NULL  |                  | 0.7665        | 0.7668        | 0.8156        | <b>0.8481</b> | <u>0.8021</u> |               |
| 55-60 |                  | IrregularMask | 0.0135        | 0.0134        | <u>0.0138</u> | 0.0129        | <b>0.0295</b> |
| 50-55 |                  |               | 0.0728        | 0.0626        | 0.0645        | <u>0.0731</u> | <b>0.0838</b> |
| 45-50 | 0.1652           |               | 0.1302        | 0.1712        | <u>0.1921</u> | <b>0.2511</b> |               |
| 40-45 | <u>0.1905</u>    |               | 0.1436        | 0.1319        | 0.1113        | <b>0.2105</b> |               |
| 35-40 | 0.1726           |               | 0.1329        | <u>0.1727</u> | 0.1248        | <b>0.1916</b> |               |
| 30-35 | <u>0.2278</u>    |               | 0.1811        | 0.1678        | 0.1553        | <b>0.2572</b> |               |
| 25-30 | 0.1956           |               | 0.1609        | 0.1216        | <u>0.1969</u> | <b>0.2237</b> |               |
| 20-25 | 0.1353           |               | 0.1935        | 0.1352        | <u>0.2157</u> | <b>0.2209</b> |               |
| 15-20 | <u>0.2015</u>    |               | 0.1869        | 0.1568        | 0.1027        | <b>0.2125</b> |               |
| 10-15 | 0.2311           |               | 0.2219        | 0.2427        | <b>0.2648</b> | <u>0.2519</u> |               |
| 5-10  | 0.2959           |               | 0.2976        | 0.3019        | <b>0.4067</b> | <u>0.3126</u> |               |
| 0-5   | 0.2616           |               | 0.2645        | 0.2678        | 0.2654        | <b>0.2742</b> |               |
| -20-0 | 0.3532           |               | 0.3607        | 0.3615        | <b>0.4362</b> | 0.3723        |               |
| NULL  | 0.7642           |               | 0.7634        | 0.8129        | <b>0.8468</b> | 0.8011        |               |

However, the boosts are lower in other ranges, which may be constrained by the characteristics of the input data. In the Irregular Mask dataset, DenMerD improves relative to the next-best model by 3.1%, 0.4%, and 2.2% over the 35-40, 15-20, and 0-5 dBZ value ranges. These performance gains are also attributed to DenMerD's dense connection modules and MD transition units, which enhance feature propagation and network depth.

Under the POD evaluation metric, DenMerD achieves significant performance improvement relative to the next best model in both datasets in the high dBZ value ranges (55-60 and 50-55), reaching 32.8% and 47.7%, respectively.

The model's performance under the SSIM metric is noteworthy, indicating a high level of restoration effectiveness and completion precision, demonstrating the

effectiveness of introducing image restoration methods into the field of weather radar beam blockage revision.

The ablation experiment is conducted on the Rectangular Mask Dataset to demonstrate the effectiveness of the Dense Connection Module and the MD Transition Unit. The objects of the ablation experiment including the RC-FCN, DenMerD wo. Dense Connection Module (DenMerD without Dense Connection Module), DenMerD wo. MD Transition Unit (DenMerD without MD Transition Unit), and the standard DenMerD. As shown in Table 5, the introduction of dense connection modules and MD transition units plays a key role in beam blockage correction under the evaluation metrics average CSI, average FAR and average POD. These three metrics are the

**Table 2** A comparative assessment of FAR

| dBZ   | Dataset          | VGG            | DenseNet      | DFNet         | RC-FCN        | DenMerD*      |               |
|-------|------------------|----------------|---------------|---------------|---------------|---------------|---------------|
| 55-60 | Rectangular Mask | <b>0.0446</b>  | 0.0645        | 0.0578        | 0.1958        | <u>0.0464</u> |               |
| 50-55 |                  | <b>0.1923</b>  | 0.2545        | 0.3253        | 0.3386        | <u>0.2089</u> |               |
| 45-50 |                  | 0.6052         | 0.5916        | 0.5575        | <u>0.4965</u> | <b>0.4814</b> |               |
| 40-45 |                  | 0.6992         | 0.6852        | 0.7001        | <u>0.6052</u> | <b>0.5965</b> |               |
| 35-40 |                  | 0.6335         | 0.6966        | 0.7585        | <u>0.6221</u> | <b>0.6088</b> |               |
| 30-35 |                  | <u>0.6321</u>  | 0.6954        | 0.6853        | 0.7172        | <b>0.6319</b> |               |
| 25-30 |                  | 0.6264         | 0.6693        | 0.7622        | <u>0.6235</u> | <b>0.6143</b> |               |
| 20-25 |                  | 0.6358         | 0.6764        | 0.6462        | <u>0.6342</u> | <b>0.6295</b> |               |
| 15-20 |                  | <u>0.6202</u>  | 0.6602        | 0.7589        | 0.7461        | <b>0.6121</b> |               |
| 10-15 |                  | 0.5857         | 0.6053        | 0.5859        | <b>0.5654</b> | <u>0.5742</u> |               |
| 5-10  |                  | 0.5203         | 0.5329        | 0.5201        | <b>0.4629</b> | <u>0.5194</u> |               |
| 0-5   |                  | 0.4859         | <u>0.4833</u> | 0.4935        | 0.4913        | <b>0.4736</b> |               |
| -20-0 |                  | <u>0.2806</u>  | 0.3412        | 0.3529        | 0.3711        | <b>0.2724</b> |               |
| NULL  |                  |                | <u>0.1685</u> | 0.1761        | 0.1777        | <b>0.0979</b> | 0.1782        |
| 55-60 |                  | Irregular Mask | 0.0478        | 0.0654        | <b>0.0453</b> | 0.1962        | <u>0.0461</u> |
| 50-55 | 0.1956           |                | 0.2549        | 0.3268        | <b>0.1948</b> | <u>0.2092</u> |               |
| 45-50 | 0.4998           |                | 0.5925        | <u>0.4871</u> | 0.6507        | <b>0.4818</b> |               |
| 40-45 | 0.6067           |                | <u>0.6023</u> | 0.7015        | 0.6991        | <b>0.5969</b> |               |
| 35-40 | 0.6349           |                | 0.6973        | 0.7592        | <u>0.6281</u> | <b>0.6095</b> |               |
| 30-35 | <u>0.6334</u>    |                | 0.6961        | 0.6868        | 0.7178        | <b>0.6323</b> |               |
| 25-30 | 0.6279           |                | 0.6703        | 0.7639        | <u>0.6153</u> | <b>0.6147</b> |               |
| 20-25 | 0.6361           |                | 0.6774        | <u>0.6329</u> | 0.7538        | <b>0.6302</b> |               |
| 15-20 | 0.6232           |                | 0.6615        | 0.7597        | <u>0.6192</u> | <b>0.6167</b> |               |
| 10-15 | 0.5869           |                | 0.6069        | 0.5863        | <b>0.5662</b> | <u>0.5756</u> |               |
| 5-10  | 0.5232           |                | 0.5331        | 0.5212        | <b>0.4633</b> | <u>0.5211</u> |               |
| 0-5   | 0.4862           |                | <u>0.4837</u> | 0.4948        | 0.4919        | <b>0.4731</b> |               |
| -20-0 | 0.2809           |                | 0.342         | 0.3539        | <u>0.2789</u> | <b>0.2737</b> |               |
| NULL  |                  |                | 0.1664        | 0.1772        | <u>0.1661</u> | <b>0.0984</b> | 0.1789        |

mean values of CSI, FAR, and POD in each dBZ range. In particular, the introduction of the Dense Connection Module fosters a more efficient propagation of information through the network, resulting in improved performance across the aforementioned metrics. Meanwhile, the MD Transition Unit demonstrates its effectiveness in further refining the correction process, leading to noteworthy improvements in the model's accuracy and reliability.

These findings underscore the crucial importance of these architectural components in addressing beam blockage challenges and highlight their potential applicability in advancing other areas of research within the domain of deep learning and meteorology. Furthermore, they provide valuable insights for future enhancements and optimizations of the DenMerD model and related techniques in real-world applications.

## Conclusion

In this paper, an edge-cloud collaborative driven deep learning model named DenMerD is proposed, which includes dense connection module and merge distribution (MD) unit. The radar sites are regarded as mobile edge nodes, and the edge-cloud collaboration is used for the correction service. The radar beam blockage correction problem is regarded as an image restoration problem. The model proposed in this paper improves 30.7% and 30.1% over the existing models in the evaluation metrics of meteorological domains such as CSI and POD, and also shows excellent performance in SSIM metrics, which proves the effectiveness of the dense connection module and MD transition unit designed in this paper in enhancing the feature propagation to improve the accuracy of the beam blockage correction, and also highlights the role of mobile edge computing

**Table 3** A comparative assessment of POD

| dBZ   | Dataset          | VGG            | DenseNet      | DFNet         | RC-FCN        | DenMerD*      |               |
|-------|------------------|----------------|---------------|---------------|---------------|---------------|---------------|
| 55-60 | Rectangular Mask | 0.0172         | 0.0163        | 0.0132        | <u>0.0189</u> | <b>0.0251</b> |               |
| 50-55 |                  | <u>0.0995</u>  | 0.0825        | 0.0875        | 0.0885        | <b>0.1099</b> |               |
| 45-50 |                  | 0.2941         | 0.2028        | 0.2534        | <u>0.2956</u> | <b>0.2986</b> |               |
| 40-45 |                  | 0.2965         | 0.2386        | 0.2357        | <u>0.2980</u> | <b>0.3089</b> |               |
| 35-40 |                  | <b>0.2770</b>  | 0.2062        | 0.2169        | 0.2215        | <u>0.2674</u> |               |
| 30-35 |                  | 0.3878         | 0.3236        | 0.3552        | <u>0.3882</u> | <b>0.3898</b> |               |
| 25-30 |                  | <u>0.3054</u>  | 0.2441        | 0.2576        | 0.2021        | <b>0.3080</b> |               |
| 20-25 |                  | 0.3565         | 0.3288        | 0.3379        | <u>0.3572</u> | <b>0.3577</b> |               |
| 15-20 |                  | <u>0.3014</u>  | 0.2965        | 0.2889        | 0.1633        | <b>0.3088</b> |               |
| 10-15 |                  | 0.3441         | 0.3284        | 0.3425        | <b>0.3631</b> | <u>0.3530</u> |               |
| 5-10  |                  | 0.4275         | 0.4425        | 0.4128        | <b>0.6029</b> | <u>0.4442</u> |               |
| 0-5   |                  | <u>0.3814</u>  | 0.3755        | 0.3749        | 0.3669        | <b>0.3951</b> |               |
| -20-0 |                  | 0.4483         | <u>0.4672</u> | 0.4442        | <b>0.5937</b> | 0.4380        |               |
| NULL  |                  | 0.8968         | 0.9053        | 0.9162        | <b>0.9354</b> | <u>0.9175</u> |               |
| 55-60 |                  | Irregular Mask | 0.0163        | 0.0156        | 0.0135        | <u>0.0172</u> | <b>0.0254</b> |
| 50-55 |                  |                | 0.0893        | 0.0819        | <u>0.0992</u> | 0.0872        | <b>0.1134</b> |
| 45-50 |                  |                | 0.2923        | 0.2011        | 0.2547        | <u>0.2965</u> | <b>0.2975</b> |
| 40-45 |                  |                | <u>0.2952</u> | 0.2375        | 0.2362        | 0.1853        | <b>0.3071</b> |
| 35-40 |                  |                | 0.2761        | 0.2060        | 0.2156        | <u>0.2788</u> | <b>0.2793</b> |
| 30-35 |                  |                | 0.3852        | 0.3234        | <u>0.3869</u> | 0.2829        | <b>0.3902</b> |
| 25-30 | 0.3041           |                | 0.2439        | <u>0.3055</u> | 0.2026        | <b>0.3077</b> |               |
| 20-25 | 0.3552           |                | 0.3277        | 0.3371        | <u>0.3557</u> | <b>0.3568</b> |               |
| 15-20 | 0.3051           |                | <u>0.3066</u> | 0.2876        | 0.1645        | <b>0.3091</b> |               |
| 10-15 | 0.3434           |                | 0.3275        | 0.3436        | <b>0.3629</b> | <u>0.3532</u> |               |
| 5-10  | 0.4267           |                | 0.4411        | 0.4134        | <b>0.6031</b> | <u>0.4438</u> |               |
| 0-5   | 0.3813           |                | 0.3742        | <u>0.3833</u> | 0.3672        | <b>0.3949</b> |               |
| -20-0 | 0.4477           |                | <u>0.4662</u> | 0.4458        | <b>0.5921</b> | 0.4372        |               |
| NULL  | 0.8965           |                | 0.9048        | 0.9169        | <b>0.9351</b> | <u>0.9188</u> |               |

**Table 4** A comparative assessment of SSIM

| Dataset          | VGG    | DenseNet | DFNet  | RC-FCN        | DenMerD*      |
|------------------|--------|----------|--------|---------------|---------------|
| Rectangular Mask | 0.7039 | 0.6854   | 0.6351 | <u>0.7422</u> | <b>0.7543</b> |
| Irregular Mask   | 0.6816 | 0.6108   | 0.6542 | <u>0.6948</u> | <b>0.7021</b> |

**Table 5** Ablation Experiment on the Rectangular Mask Dataset

| Model                | CSI-AVG       | FAR-AVG       | POD-AVG       |
|----------------------|---------------|---------------|---------------|
| RC-FCN               | 0.2487        | 0.4977        | 0.3497        |
| wo. Dense Connection | 0.2579        | 0.4852        | 0.3488        |
| wo. MD Unit          | 0.2543        | 0.4712        | 0.3475        |
| DenMerD              | <b>0.2644</b> | <b>0.4605</b> | <b>0.3516</b> |

in processing large-scale meteorological data. Future research could explore how to further optimise the performance of the model, including improving the

design of the dense connection module and MD units to accommodate a wider range of meteorological data characteristics. In addition, the model's edge-cloud collaboration approach can be applied to other areas such as radar echo extrapolation, semantic segmentation, etc. for wider real-time data processing and decision support.

**Acknowledgements**

This work has received funding from National Key Research and Development Program of China under Grant No.2021YFE0116900, National Natural Science Foundation of China (No. 42275157, 62002276 and 41975142).

**Authors' contributions**

Qi Liu and Jiawei Sun gave the main idea of this paper. All authors took part in the discussion and the proposal of the work described in this paper. Jiawei Sun wrote the Introduction, Related work, and Method sections. Yonghong Zhang and Xiaodong Liu wrote the rest of sections. All authors reviewed the manuscript.

**Funding**

This work has received funding from National Key Research and Development Program of China under Grant No.2021YFE0116900, National Natural Science Foundation of China (No. 42275157, 62002276 and 41975142).

**Availability of data and materials**

Not applicable.

**Declarations****Ethics approval and consent to participate**

Not applicable.

**Consent for publication**

Not applicable.

**Competing interests**

The authors declare no competing interests.

Received: 7 November 2023 Accepted: 30 January 2024

Published online: 05 February 2024

**References**

- Li N, Wang Z, Sun K, Chu Z, Leng L, Lv X (2017) A quality control method of ground-based weather radar data based on statistics. *IEEE Trans Geosci Remote Sens* 56(4):2211–2219
- Yang Z, Liu Q, Wu H, Liu X, Zhang Y (2022) Cema-lstm: enhancing contextual feature correlation for radar extrapolation using fine-grained echo datasets. *Comput Model Eng Sci* 135(1):45–64
- Yang Z, Wu H, Liu Q, Liu X, Zhang Y, Cao X (2023) A self-attention integrated spatiotemporal lstm approach to edge-radar echo extrapolation in the internet of radars. *ISA Trans* 132:155–166
- Awaka J, Le M, Chandrasekar V, Yoshida N, Higashiawatoko T, Kubota T, Iguchi T (2016) Rain type classification algorithm module for gpm dual-frequency precipitation radar. *J Atmos Ocean Technol* 33(9):1887–1898
- Lin H, Xu X, Bilal M, Cheng Y, Liu D (2023) Intelligent retrieval of radar reflectivity factor with privacy protection under meteorological satellite remote sensing. *IEEE J Sel Top Appl Earth Obs Remote Sens* 16:6948–6957
- Omrani E, Sharif HO (2018) Evaluation of the global precipitation measurement (gpm) satellite rainfall products over the lower colorado river basin, texas. *JAWRA J Am Water Resour Assoc* 54(4):882–898
- Xiao Y, Wan Y, Wang Z (2016) Quality control of dual prf velocity data for doppler weather radars. *Plateau Meteorol* 35(4):1112–1122
- Hu S, Zhang Y, Deng W, Chen X (2014) Correction schemes for radar blockage by complex terrain at shenzhen and validation. *J Trop Meteorol* 30(1):1–10
- Huang G, Liu Z, Van Der Maaten L, Weinberger KQ (2017) Densely connected convolutional networks. In: *Proceedings of the IEEE conference on computer vision and pattern recognition*. IEEE, Honolulu, p 4700–4708
- Tian H, Xu X, Lin T, Cheng Y, Qian C, Ren L, Bilal M (2022) Dima: Distributed cooperative microservice caching for internet of things in edge computing by deep reinforcement learning. *World Wide Web* 25(5):1769–1792
- Leyva-Mayorga I, Martinez-Gost M, Moretti M, Pérez-Neira A, Vázquez MÁ, Popovski P, Soret B (2023) Satellite edge computing for real-time and very-high resolution earth observation. *IEEE Trans Commun* 71(10):6180–6194
- Yao L, Xu X, Bilal M, Wang H (2022) Dynamic edge computation offloading for internet of vehicles with deep reinforcement learning. *IEEE Trans Intell Transp Syst* 24(11):12991–12999
- Qi L, Song H, Zhang X, Srivastava G, Xu X, Yu S (2021) Compatibility-aware web api recommendation for mashup creation via textual description mining. *ACM Trans Multimed Comput Commun Appl* 17(1s):1–19
- Liu S, Deng W (2015) Very deep convolutional neural network based image classification using small training sample size. In: *2015 3rd IAPR Asian conference on pattern recognition (ACPR)*. IEEE, Nanjing, p 730–734
- Wang W, Wang Z, Zhou Z, Deng H, Zhao W, Wang C, Guo Y (2021) Anomaly detection of industrial control systems based on transfer learning. *Tsinghua Sci Technol* 26(6):821–832
- Du J, Xu M, Gill SS, Wu H (2023) Computation energy efficiency maximization for intelligent reflective surface-aided wireless powered mobile edge computing. *IEEE Trans Sustain Comput* 1–15
- Xu X, Yang C, Bilal M, Li W, Wang H (2022) Computation offloading for energy and delay trade-offs with traffic flow prediction in edge computing-enabled iov. *IEEE Trans Intell Transp Syst* 24(12):15613–15623
- Ding J, Han L, Li J, Zhang D (2023) Resource allocation strategy for blockchain-enabled NOMA-based MEC networks. *J Cloud Comp* 12:142. <https://doi.org/10.1186/s13677-023-00497-5>
- Yan H, Xu X, Dai F, Qi L, Zhang X, Dou W (2022) Service caching for meteorological emergency decision-making in cloud-edge computing. In: *2022 IEEE International Conference on Web Services (ICWS)*. IEEE, Barcelona, p 120–128
- Mu L, Ge B, Xia C, Wu C (2023) Deep reinforcement learning based adaptive threshold multi-tasks offloading approach in mec. *Comput Netw* 232:109803
- Li Z, Xu X, Cao X, Liu W, Zhang Y, Chen D et al (2022) Integrated cnn and federated learning for covid-19 detection on chest x-ray images. *IEEE/ACM Trans Comput Biol Bioinforma* 1–11
- Xu X, Gu J, Yan H, Liu W, Qi L, Zhou X (2022) Reputation-aware supplier assessment for blockchain-enabled supply chain in industry 4.0. *IEEE Trans Ind Inform* 19(4):5485–5494
- Yang Y, Lou K, Wang E, Liu W, Shang J, Song X et al (2023) Multi-agent reinforcement learning based file caching strategy in mobile edge computing. *IEEE/ACM Trans Netw* 31(6):3159–3174
- Xu X, Tang S, Qi L, Zhou X, Dai F, Dou W (2023) Cnn partitioning and offloading for vehicular edge networks in web3. *IEEE Commun Mag* 61(8):36–42
- Wang X, Li J, Ning Z, Song Q, Guo L, Guo S et al (2023) Wireless powered mobile edge computing networks: a survey. *ACM Comput Surv* 55(13s):1–37
- Zhang Y, Cheng M (2011) Dynamical weather radar beam blockage correction. In: *2011 International Conference on Computer Distributed Control and Intelligent Environmental Monitoring*. IEEE, Changsha, p 67–70
- Chen W, He J, Shi Z, Ma J, Lin Q (2020) Application of dem-based beam occlusion correction in radar quantitative estimation of precipitation. *Meteorol Sci Technol* 48(1):9–14
- Liu Y, Li C, Zhang L, Wen H, Wang S (2020) Statistical analysis of terrain blockage impacts on the cinrad network based on dem data. *Acta Meteorol Sin* 78(4):705–720
- Gou Y, Wang Z, Liu L, Duan Y, Chen C (2017) Application and evaluation of radar partial blockage identification. *Plateau Meteorol* 36(1):229–240
- Huang X, Ma L, Yang M, Yin J, Liu Y (2019) Recognition and correction of beam blockage of weather radar based on spatial correlation. *J Meteorol Sci* 39(4):532–539
- Wang G, Ping F, Yang M, Pang Q (2019) A radar echo quality control method based on climate statistical analysis. *Meteorol Sci Technol* 47(1):19–28
- Mao Y, Zhang T, Fu B, Thanh DN (2022) A self-attention based wasserstein generative adversarial networks for single image inpainting. *Pattern Recog Image Anal* 32(3):591–599
- Phutke SS, Murala S (2022) Pseudo decoder guided light-weight architecture for image inpainting. *IEEE Trans Image Process* 31:6577–6590
- Ma Y, Liu X, Bai S, Wang L, Liu A, Tao D et al (2022) Regionwise generative adversarial image inpainting for large missing areas. *IEEE Trans Cybern* 53(8):5226–5239
- Quan W, Zhang R, Zhang Y, Li Z, Wang J, Yan DM (2022) Image inpainting with local and global refinement. *IEEE Trans Image Process* 31:2405–2420
- Aishwarya G, Krishnan KR (2021) Generative adversarial networks for facial image inpainting and super-resolution. In: *Journal of Physics: Conference Series*, vol 2070. IOP Publishing, India, p 012103
- Nazeri K, Ng E, Joseph T, Qureshi FZ, Ebrahimi M (2020) Edgeconnect: generative image inpainting with adversarial edge learning. *arXiv preprint arXiv:1901.00212*
- Hong X, Xiong P, Ji R, Fan H (2019) Deep fusion network for image completion. In: *Proceedings of the 27th ACM international conference on multimedia*. ACM, Nice, p 2033–2042
- Wu H, Liu Q, Liu X, Zhang Y, Xu X, Bilal M (2021) A fcn approach to blockage correction in radars. In: *2021 IEEE Intl Conf on Dependable, Autonomic and Secure Computing, Intl Conf on Pervasive Intelligence and Computing, Intl Conf on Cloud and Big Data Computing, Intl Conf on Cyber Science and Technology Congress (DASC/PiCom/CBDCom/CyberSciTech)*. IEEE, AB, Canada, p 482–487

40. Wu H, Liu Q, Liu X, Zhang Y, Yang Z (2022) An edge-assisted cloud framework using a residual concatenate fcn approach to beam correction in the internet of weather radars. *World Wide Web* 25(5):1923–1949
41. Li Z, Xu X, Hang T, Xiang H, Cui Y, Qi L et al (2022) A knowledge-driven anomaly detection framework for social production system. *IEEE Trans Comput Soc Syst* 1–14
42. Yan H, Bilal M, Xu X, Vimal S (2022) Edge server deployment for health monitoring with reinforcement learning in internet of medical things. *IEEE Trans Comput Soc Syst* 1–11
43. Ning Z, Hu H, Wang X, Guo L, Guo S, Wang G et al (2023) Mobile edge computing and machine learning in the internet of unmanned aerial vehicles: a survey. *ACM Comput Surv* 56(1):1–31
44. Chai F, Zhang Q, Yao H, Xin X, Gao R, Guizani M (2023) Joint multi-task offloading and resource allocation for mobile edge computing systems in satellite iot. *IEEE Trans Veh Technol* 72(6):7783–7795
45. Chen Y, Zhao J, Hu J, Wan S, Huang J (2023) Distributed task offloading and resource purchasing in noma-enabled mobile edge computing: hierarchical game theoretical approaches. *ACM Trans Embed Comput Syst* 23(1):1–28
46. Zhang W, Luo J, Chen L, Liu J (2023) A trajectory prediction-based and dependency-aware container migration for mobile edge computing. *IEEE Trans Serv Comput* 16(5):3168–3181

### **Publisher's Note**

Springer Nature remains neutral with regard to jurisdictional claims in published maps and institutional affiliations.